PROCEEDINGS OF THE 18TH NORTH AMERICAN MINE VENTILATION SYMPOSIUM
(NAMVS 2021), JUNE 12-17, 2021, RAPID CITY, SOUTH DAKOTA, USA

Mine Ventilation

Editor

Purushotham Tukkaraja, Ph.D., QP

Mining Engineering & Management, South Dakota Mines, Rapid City, SD, USA

CRC Press
Taylor & Francis Group
Boca Raton London New York

CRC Press is an imprint of the
Taylor & Francis Group, an **informa** business

A BALKEMA BOOK

CRC Press/Balkema is an imprint of the Taylor & Francis Group, an informa business

Typeset by Integra Software Services Pvt. Ltd., Pondicherry, India

Library of Congress Cataloging-in-Publication Data

A catalog record has been requested for this book

Published by: CRC Press/Balkema
Schipholweg 107C, 2316 XC Leiden, The Netherlands
e-mail: enquiries@taylorandfrancis.com
www.routledge.com – www.taylorandfrancis.com

ISBN: 978-1-032-03679-3 (Hbk)
ISBN: 978-1-032-03681-6 (Pbk)
ISBN: 978-1-003-18847-6 (eBook)
DOI: 10.1201/9781003188476

NAMVS 2021 – Tukkaraja (Ed.)

Comparison of mineral content in respirable coal mine dust samples estimated using FTIR, TGA, and SEM-EDX

N. Pokhrel, E. Agioutanti, C. Keles, S. Afrouz & E.A. Sarver
Virginia Polytechnic Institute and State University, Blacksburg, Virginia, USA

ABSTRACT: Since the mid-1990s, there has been a resurgence of severe lung disease among US coal miners. This has prompted efforts to better characterize and monitor respirable dust exposures—especially with respect to mineral content sourced from rock strata surrounding the coal, which is believed to play a central role in many cases of disease. Recently, a rapid analysis method for silica (quartz) has been developed using direct-on-filter Fourier-transform infrared (FTIR) spectroscopy. It can also be used to determine kaolinite, presumably a primary silicate mineral in many coal mines. Other methods, including thermogravimetric analysis (TGA) and scanning electron microscopy with energy dispersive x-ray (SEM-EDX), can also be used to estimate mineral content in respirable coal mine dust. However, there have been few efforts to compare results across multiple methods. This study compares estimates of mineral content derived from FTIR, TGA, and SEM-EDX on respirable dust samples collected in 16 underground coal mines across the US.

1 INTRODUCTION

Exposure to respirable dust has long been recognized as an occupational health hazard to coal mine workers (IARC, 1997; NASEM, 2018). Respirable crystalline silica (RCS) contained in the dust can be particularly hazardous (Castranova and Vallyathan, 2000; Laney and Weissman, 2014; Schatzel, 2009). Indeed, RCS has been cited as a likely causal factor in a dramatic resurgence of severe and rapid lung diseases among coal miners in central Appalachia over the past two decades (Almberg et al., 2018; Blackley et al., 2016; CDC, 2006). This has renewed efforts to improve RCS monitoring in coal mines (Ashley et al., 2020; Cauda et al., 2016; Miller et al., 2013). Moreover, based on knowledge gaps surrounding the whole composition of respirable coal mine dust, and its variability with different geologic and mining conditions, there have been calls to better characterize the dust in general (NASEM, 2018).

Traditionally, measurement of silica in US coal mines is done using the MSHA P7 Standard Method (MSHA, 2008). It uses infrared spectroscopy (IR) to analyze the quartz mass in a dust sample, following ashing of the sample filter. (It is noted that quartz is well established as the primary form of crystalline silica in coal mine environments, and the terms quartz and silica are often used interchangeably.) However, because of the sample preparation and equipment required for the P7 analysis, it is practically limited to centralized labs. This translates to considerable lag time (days to weeks) between sample collection and reporting of results—which impedes swift mitigation of hazardous exposure conditions (Cauda et al., 2016; Miller et al., 2012).

To address this issue, the US National Institute for Occupational Safety and Health (NIOSH) has been working to develop a new direct-on-filter (DOF) approach for quartz measurement (Cauda et al., 2016; Miller et al., 2012; Miller et al., 2013; Miller et al., 2017). Like Method P7, this method analyzes the quartz in a filter sample. While it is not a real-time

DOI: 10.1201/9781003188476-27

measurement, it requires no sample preparation and uses a portable Fourier-transform infrared (FTIR) instrument, such that the analysis can be done immediately after sample collection. Miller et al. found strong linear correlations (ranging from 0.90 – 0.97) between DOF and P7-derived quartz data, demonstrating its potential as an end-of-shift method (Miller et al., 2012).

Although the primary focus of the DOF-FTIR method has been on quartz measurement, it has the potential to provide broader insights to the range of mineral constituents that make up respirable coal mine dust (Cauda et al., 2016; Miller et al., 2017). Similar to determination of quartz from its characteristic peaks in the FTIR spectrum, other minerals can also be identified and possibly quantified from the spectrum. In fact, kaolinite, which is generally expected to be one of the predominant silicate minerals in many coal mine environments (Schatzel, 2009; Su et al., 2020), is already an integral part of the quartz quantification method; kaolinite has an overlapping peak with quartz, and this interference is quantified (in terms of spectrum peak area) in order to analytically correct the quartz measurement (Cauda et al., 2016; Lee et al., 2013; Miller et al., 2012). Thus, kaolinite mass (K), along with quartz (Q), can be easily reported from the DOF-FTIR analysis of coal mine dust samples using calibration curves for each analyte. It is possible that other minerals of interest can be reported too (e.g., calcite, which could serve as crude surrogate for respirable dust sourced from limestone rock dusting products being used in a mine).

In addition to FTIR, other analytical methods can also be used to characterize respirable coal mine dust. Thermogravimetric analysis (TGA) is a mass-based method that the authors' research group recently applied to determine coal, non-carbonate minerals, and carbonates fractions of dust, which can be loosely associated with dust sources related to coal cutting, rock strata cutting/drilling, and rock dust application, respectively, in many mines (Agioutanti et al., 2020). TGA basically tracks the weight change of a sample with temperature in a controlled environment. Since coal, carbonates, and non-carbonates have their own thermal behavior (i.e., coal and carbonates tend to lose mass in characteristic temperature regions, while the non-carbonate minerals of interest like silica and silicates tend to be inert in those regions), the sample behavior can be used to estimate these three primary fractions (Agioutanti et al., 2020). Further, if rock-strata sourced dust in a coal mine is dominated by silica and silicates, the non-carbonate minerals fraction might be comparable to the Q+K per the FTIR (Table 1).

Scanning electron microscopy with energy dispersive X-ray (SEM-EDX) analysis is a particle-based method that can be used to size and classify individual particles. For respirable coal mine dust, the authors' group has established routines to bin particles into the following predefined mineralogy classes: carbonaceous (C) and mixed carbonaceous (MC), which are generally associated with coal dust and/or diesel particulates (in the very fine sizes); alumino-silicates (AS, which can be further sub-classified as either kaolinite ASK, or other alumino-silicates, ASO), other silicates (SLO), silica (S), and metal oxides and sulfides (M), which are generally associated with rock-strata sourced dust; carbonates (CB), which are associated with rock dust (e.g., limestone) application in most US mines; and others (O), which are particles not otherwise classified (Johann-Essex et al., 2017b; Sarver et al., 2019). It stands to reason that distribution of dust across these classes might also be comparable to FTIR and TGA measures per Table 1.

Table 1. Comparable constituents across each of the three methods.

	Comparison of constituents attributed to likely sources				
Method	rock strata			rock dust products	coal
FTIR	Q	K	$Q + K$	-	-
TGA	-	-	non-carbonate minerals	carbonates	coal
SEM-EDX	S	ASK	S + ASK + ASO + SLO + M	CB	C + MC

Though FTIR, TGA, and SEM-EDX can all be used to measure certain constituents of respirable coal mine dust, they have not been directly compared. The primary goal of the current study is to compare mineral content, specifically, estimated using all three methods. For this, samples from different locations in 16 underground US coal mines were analyzed. Notably, the study also represents an early application of the DOF-FTIR method for dust characterization research.

2 MATERIALS AND METHODS

2.1 *Sample collection*

Respirable dust samples were collected in 2018 from 16 different US underground coal mines (numbered 10-25), representing five mine regions: northern Appalachia (NA, mines 7-9), central Appalachia (CA, mines 10-15, 21, 22, 25), western coal basin (W, mines 23 and 24), and mid-western Illinois coal basin (MW, mines 19 and 20). A total of 93 sets of samples (each containing multiple replicates) were collected in several key locations in each mine: near the coal 'feeder (F)' or along the main conveyor belt; near the 'intake (I)' (including near the headgate of a longwall); near major 'production (P)' activities (i.e. downwind of a continuous miner or along the longwall face); in the 'bolter (B)' (i.e. just downwind of an active roof-bolter); and in the 'return (R)' (including near the tailgate of a longwall). Each sample set was collected over about 2-4 hours.

Escort ELF air sampling pumps with a 10-mm nylon Dorr-Oliver cyclone at a flow rate of 2.0 lpm (yielding a d50 of about 3.5 μm) were used to collect dust onto 37-mm filters in two-piece styrene cassettes. For the FTIR analysis, the samples were collected onto polyvinyl chloride filters (PVC, 5.0 μm pore size), while for SEM and TGA, polycarbonate filters (PC, 0.4 μm pore size) were used (Agioutanti et al., 2020; Johann-Essex et al., 2017a; Sarver et al., 2019). The PVC filters were pre- and post-weighed using a microbalance (Sartorius MSE6.6S, Gottingen, Germany) to determine the total dust mass.

2.2 *FTIR analysis*

For each sample set, one PVC filter was prepared for analysis by an ALPHA II FTIR Spectrometer (Bruker optics, Billerica, MA) to get the absorbance spectra between spatial frequencies of 4000 cm^{-1} to 400 cm^{-1}. The PVC filters were carefully taken out from the 2-piece cassettes and placed onto FTIR-compatible 4-piece cassettes (Zefon International, Ocala, FL), which were then mounted centrally onto a sample holder within the chamber of the FTIR instrument. Sixteen scans of the center 6-mm diameter spot on each filter were taken at a resolution of 4 cm^{-1} using Blackman-Harris three-term apodization, which then underwent a rubber band baseline correction with 64 baseline points (to remove distortions) (Miller et al., 2012; Miller et al., 2017).

Being a direct-on-filter approach, the FTIR spectra obtained on a dust sample also includes the absorbance data of the filter material. This was addressed by subtracting the background spectrum of a blank PVC filter. Blank filter data was obtained for each batch of dust samples analyzed by FTIR to ensure that any effect of environmental conditions (e.g., humidity) was minimized.

In an absorbance spectrum for a pure sample, quartz appears as a doublet peak at 780 and 800 cm^{-1}, while kaolinite appears as a larger peak at 915 cm^{-1} and a smaller peak at 790 cm^{-1}. Using Bruker's OPUS software (Version 8.2.28, 32 bit), the spectral region between 816-767 cm^{-1} (corresponding to the doublet peak for Q) and between 930-900 cm^{-1} (corresponding to the larger peak for K) was integrated to find the peak areas, using calculations consistent with other IR methods for quartz analysis (Miller et al., 2012; MSHA, 2008). Since the smaller peak of K lies in the same range for quartz doublet peak, the Q peak area was corrected for this interference using a previously calculated correction ratio

of 3.8 for the FTIR instrument (Miller et al., 2012; Miller et al., 2017). This was done using the following equation (Miller et al., 2012):

$$Corrected\ Q\ peak\ area = Q\ peak\ area - \frac{K\ peak\ area}{3.8}$$

These peak areas of the 6-mm spot on the filter center were extrapolated to determine the total Q and K masses on the entire 37-mm filter. This was done using previously established calibration curves developed by NIOSH from regression analysis of the peak integrated area versus the gravimetric mass of pure crystalline silica (Min-U-Sil 5), kaolinite, or a mixture of the two aerosolized in a calm-air laboratory dust chamber (Cauda et al., 2016; Miller et al., 2017; NIOSH, 2019). It is important to note that those calibration curves were developed with samples collected in 3-piece cassettes (again using 10-mm nylon Dorr-Oliver cyclones at 2 LPM flowrate). Since the mine samples used in this study were collected in 2-piece cassettes—which promote a slightly different dust loading pattern—the FTIR-derived Q and K mass results were also corrected using a previously established correction factor of 0.877 (Miller et al., 2013). Finally, the quantified masses were converted to mass percentages using total mass of the samples.

2.3 *TGA analysis*

One PC filter from each sample set was used for TGA per Agioutanti et al. (2020). Briefly, dust was recovered from the sample filters by sonication in isopropanol, redeposited in a clean, tared sample pan, and analyzed by a Q500 Thermogravimetric Analyzer (TA Instruments, New Castle, DE) using the prescribed thermal ramping routine. (Notably, the same instrument used by Agioutanti et al. was used here.) Agioutanti et al. showed that weight change in several regions of interest could be used to estimate the coal, carbonates, and non-carbonate minerals mass fractions in the sample; and published a series of mass balance equations that can be applied to a sample thermogram for this purpose. These were applied to all sample thermograms here.

2.4 *SEM-EDX analysis*

Finally, one PC filter from each sample set was also analyzed by the SEM-EDX. Dust samples were prepared and analyzed based on a previously established method in Sarver et al. (2019), with a computer-controlled routine using an FEI Quanta 600 FEG environmental scanning electron microscope (ESEM) (Hillsboro, OR, USA) equipped with a backscatter electron detector (BSD) and a Bruker Quantax 400 EDX spectroscope (Ewing, NJ, USA) (Johann-Essex et al., 2017a; Johann-Essex et al., 2017b; Sarver et al., 2019). This routine, using Bruker's Esprit software (Version 1.9.4), was used to scan multiple areas across each sample in order to analyze about 800 particles per sample. For each particle, the long and intermediate dimensions were recorded, and its elemental spectra were used to classify its mineralogy (Table 2). These data were then used to estimate the particle's mass. The volume was calculated using the long and intermediate dimensions of the particle and its assumed thickness (or short dimension); assumptions for short-to-intermediate dimension ratio (SI) and specific gravity (SG) are shown in Table 2 for each class. Computed particle masses in each class were summed and divided by the total particle mass for the sample to estimate the mass fraction (%) for each class, which were then compared to the FTIR and TGA results.

3 RESULTS AND DISCUSSION

Table 3 summarizes the FTIR, TGA, and SEM-EDX results from all 93 sets of respirable mine dust samples included in the study. It is noted that the TGA recovered mass refers to the sum of the coal, carbonates, and non-carbonate minerals masses determined for each PC

Table 2. SEM-EDX classification criteria for supramicron particles, along with assumptions for S:I ratio and SG for each mineralogy class (updated from Johann-Essex et al., 2017b).

	Atomic %								Particle size to mass assumptions	
Class	O	Al	Si	C	Mg	Ca	Ti	Fe	SI	SG
C	<29	≤0.3	≤0.3	≥75	≤0.5	≤0.41	≤0.06	≤0.15	0.6	1.4
MC		≤0.35	<0.35		≤0.5	≤0.5	≤0.6	≤0.6	0.6	1.4
ASK[1]		≥0.35 (≥39)	≥0.35 (≥32)		(<15)	(<8)	(<13)	(<13)	0.4	2.6
ASO[1]		≥0.35 (<39)	>0.35 (<32)		(≥15)	(≥8)	(≥13)	(≥13)	0.4	2.6
SLO[2]			≥0.33						0.4	2.6
S[3]			≥0.33						0.7	2.65
M		>1					>1	>1	0.7	4.96
CB	>9				>0.5	>0.5			0.7	2.7

1 To differentiate ASK from ASO, additional limits for Al, Si, Mg, Ca, Ti and Fe are shown in parenthesis (normalized to exclude C and O)
2 Additional limits for SLO: Si/(Al+Si+Mg+Ca+Ti+Fe) < 0.5
3 Additional limits for S: Al/Si < 1/3 and Si/(Al+Si+Mg+Ca+Ti+Fe) ≥ 0.5

sample analyzed. However, this may not match the total sample mass for the paired PVC filter due to several factors including differences in total mass collected on each filter (i.e., due to differences in the filter media themselves or spatial variation in the sampling environment), and less than 100% recovery of dust from the PC filter. That said, PVC sample mass and TGA recovered mass do generally trend together.

The sample mass (determined from the PVC filters in each set) was generally highest in the P and R sampling locations (mean values of 0.75 and 1 mg, respectively), while masses in the I, B, and F locations were lower (means of 0.2, 0.3, and 0.3 mg, respectively). It is worth noting that sample masses reported here should not be used as a proxy for mass concentration in the sampling location since the sampling time varied. However, the sample mass does have important ramifications for each analytical method. For SEM-EDX, high-mass samples may exhibit dense loading on the filter, which can challenge analysis of individual particles. Though no mass limit has been established, care was taken to avoid analysis on filter areas that may have had overlapping particles. Even so, it is possible that elemental spectra on some particles were influenced by surrounding particles.

For TGA, Agioutanti et al. (2020) found that limits of detection (LOD) and quantification (LOQ) in lab-generated respirable dust samples were on the order of 50 and 150 μg, respectively, of recovered dust for each primary sample component (i.e., coal, carbonate, or non-carbonates). In real mine dust samples, it is impossible to know the component masses *a priori*—rather only the total recovered dust mass is known. Given that the current study represents the first time this TGA method has been used for mine dust samples, LOD and LOQ were not applied strictly here. However, results for particularly low-mass samples should be considered with some caution. (E.g., Using a threshold of 200 μg total recovered dust, about 40 samples per Table 3 would be considered low-mass).

Similarly, FTIR results can also be affected by sample mass, and only the total dust mass (on PVC filter) is known *a priori*. Per Cauda et al. (2016), the LOD and LOQ for Q are 5 and 16 μg, respectively; and using the same approach to compute LOD and LOQ, the values for K was estimated as 44 and 147 μg, respectively. As shown in Table 3, only 27 of the 93 samples had quantifiable Q, with 5 samples between LOD and LOQ, and the rest of them were below LOD (and had total sample mass <350μg). In contrast, 64 of the samples had quantifiable K, and the rest were between LOD and LOQ, with the exception of one sample below LOD.

Table 3. Summary of results for 93 sets of respirable coal mine dust samples.

Samp. No.	Mine		Samp. Loc.	PVC Sample Mass (mg)	TGA Recovered Mass (mg)	FTIR (mass %)		TGA (mass %)			SEM-EDX (mass %)							
	Reg.	No.				Q	K	Coal	Carb.	Non-carb.	C	MC	ASK	ASO	S	SLO	M	CB
1	SCA	10	B	0.148	0.146		24.7	25.4	3.7	70.9	17.8	16.6	25.7	32.7	5.6	0.0	0.8	0.8
2	SCA	10	B	0.181	0.198		26.4	26.8	5.5	67.7	3.8	8.9	47.1	35.3	3.7	0.0	0.3	1.0
3	SCA	10	F	0.132	0.157		23.6	41.7	3.5	54.8	11.3	7.9	32.3	35.3	8.3	0.0	3.9	0.9
4	SCA	10	F	0.183	0.064		18.3	43.6	16.8	39.6	8.3	7.7	37.0	44.2	1.0	0.0	2.0	0.0
5	SCA	10	I	0.005	0.049		n/a*	84.4	1.8	13.7	22.6	14.0	5.4	9.1	41.0	1.3	0.4	6.2
6	SCA	10	P	0.089	n/a		29.9	n/a	n/a	n/a	n/a	n/a	n/a	n/a	n/a	n/a	n/a	n/a
7	SCA	10	P	1.494	1.286		21.3	22.7	3.2	74.1	0.0	0.0	83.5	15.8	0.7	0.0	0.0	0.0
8	SCA	10	R	0.038	0.074		38.1*	62.3	3.3	34.4	28.0	13.2	23.8	24.9	8.3	0.2	0.3	1.3
9	SCA	11	B	0.106	0.042		24.4	36.0	9.3	54.7	1.2	5.2	11.8	60.4	14.2	0.2	1.2	5.8
10	SCA	11	F	0.164	0.104		14.2	54.4	6.9	38.7	23.5	10.8	11.2	30.0	11.1	0.0	7.8	5.6
11	SCA	11	P	1.153	0.666	6.2	11.9	11.4	4.9	83.7	0.0	0.1	3.8	95.4	0.8	0.0	0.0	0.0
12	SCA	11	R	0.749	0.137	6.7	13.9	25.8	5.2	69.0	0.0	0.0	1.8	97.5	0.7	0.0	0.0	0.0
13	SCA	12	B	0.103	0.031		21.0	55.1	13.4	31.4	32.1	16.5	9.7	19.0	4.2	1.0	1.4	16.1
14	SCA	12	I	0.054	0.074		35.3	76.0	5.4	18.6	56.7	8.2	7.0	11.7	5.3	0.0	0.0	11.1
15	SCA	12	P	1.077	0.486	4.0	12.8	29.5	4.8	65.6	7.0	7.5	29.6	52.0	3.4	0.0	0.4	0.0
16	SCA	12	R	0.649	0.430	3.2	15.3	20.8	7.4	71.7	0.1	0.6	7.2	91.3	0.7	0.0	0.0	0.1
17	SCA	13	B	2.535	3.405	12.3	10.1	13.6	5.8	80.6	0.0	0.0	2.1	96.8	1.1	0.0	0.0	0.0
18	SCA	13	F	0.189	0.057		8.4*	78.0	8.1	14.0	36.1	8.4	2.1	7.6	1.1	2.2	1.2	41.2
19	SCA	13	I	0.035	0.030		43.2*	39.9	26.8	33.3	6.5	1.0	1.3	5.7	1.4	0.1	0.0	84.1
20	SCA	13	I	0.701	0.125	4.6	5.9	62.9	12.8	24.4	23.1	10.5	3.7	41.3	7.0	0.0	0.3	14.0
21	SCA	13	R	7.347	11.346	4.7	1.5	8.1	69.5	22.4	0.0	0.0	0.0	9.5	0.0	5.4	0.0	85.0
22	SCA	13	R	1.297	1.312	1.8	2.6	73.9	4.4	21.7	58.9	10.8	5.4	15.4	4.1	0.0	0.1	5.4
23	SCA	14	B	0.039	0.055		42.8*	29.0	12.5	58.6	10.5	6.9	27.9	32.2	16.6	0.0	2.6	3.2
24	SCA	14	F	0.187	0.213		19.1	27.5	5.1	67.4	2.3	4.5	10.6	53.3	13.2	2.1	1.4	12.7
25	SCA	14	I	0.002	0.055		n/a*	66.7	9.2	24.1	8.6	3.8	4.3	16.8	8.7	0.0	0.0	57.9
26	SCA	14	P	4.348	3.682	7.3	11.3	9.5	4.7	85.8	0.0	0.0	2.0	97.9	0.1	0.0	0.0	0.0
27	SCA	21	B	0.085	0.029		20.5*	46.5	10.2	43.3	4.7	8.4	7.9	37.2	15.1	0.1	1.2	25.4

Tab.3 (Continued)

28	SCA	21	F	0.089	0.030		21.0	15.8	2.8	81.5	6.3	10.1	15.9	47.9	11.8	0.0	3.3	4.6
29	SCA	21	I	0.063	0.064		27.6*	60.8	5.6	33.6	7.8	8.7	18.4	42.8	10.1	0.0	2.0	10.1
30	SCA	21	P	1.415	1.757	5.2	12.0	8.1	4.1	87.9	0.0	0.0	1.5	98.1	0.4	0.0	0.0	0.0
31	SCA	21	R	0.557	1.086	4.4	12.8	8.7	4.2	87.1	0.0	0.0	5.4	93.7	0.8	0.0	0.0	0.0
32	SCA	22	F	0.018	0.021		78.1*	61.9	5.2	33.0	40.0	10.6	3.9	9.7	6.3	0.0	26.5	3.0
33	SCA	22	I	0.003	0.003		n/a*	89.7	6.3	4.1	40.3	11.6	9.5	19.3	8.8	0.0	1.3	9.2
34	SCA	22	P	1.230	0.339	7.0	7.2	34.2	16.3	49.5	0.0	0.0	0.5	98.2	1.3	0.0	0.0	0.0
35	SCA	25	B	0.416	0.286	8.65	21.7	39.0	6.1	54.9	0.0	0.3	18.0	76.7	5.0	0.0	0.0	0.0
36	SCA	25	F	0.336	0.460	5.63	13.0	40.3	8.3	51.8	2.7	7.5	9.6	64.2	6.7	0.2	2.5	6.6
37	SCA	25	I	0.010	0.026			77.4	0.7	21.8	7.2	9.1	17.3	43.0	8.6	1.1	1.2	12.5
38	SCA	25	P	0.357	0.191	4.24	19.2	57.3	6.1	36.6	0.5	3.9	15.7	71.0	5.3	0.0	0.7	3.0
39	SCA	25	P	0.189	0.186	4.65	20.8	18.4	7.2	74.4	6.9	11.1	32.6	31.5	12.2	0.0	5.5	0.1
40	SCA	25	P	0.669	0.354	5.59	19.6	42.3	1.0	56.7	0.0	0.7	37.4	59.5	2.1	0.1	0.2	0.0
41	SCA	25	P	0.311	0.064	5.48	21.8	26.9	9.8	63.3	1.9	7.5	23.4	50.0	4.8	0.0	0.8	11.7
42	SCA	25	P	0.227	0.060	3.10	19.8	29.1	1.1	69.8	2.9	6.3	35.9	42.3	7.7	0.1	2.4	2.3
43	SCA	25	P	0.088	0.046	2.62	22.3	42.7	8.3	49.0	6.3	8.8	33.7	28.3	9.1	0.0	2.2	11.7
44	SCA	25	P	0.949	0.330	7.29	19.1	13.9	7.6	78.5	0.0	0.1	28.6	69.7	1.6	0.0	0.0	0.0
45	SCA	25	P	0.596	0.255	7.00	20.2	13.8	5.1	81.1	0.1	0.1	26.5	71.1	0.7	0.0	0.0	1.5
46	SCA	25	R	0.130	0.110	2.41	15.3	22.1	6.2	71.6	11.5	12.6	24.1	24.9	13.7	0.0	0.8	12.4
47	SCA	25	R	0.132	0.021	4.43	24.3	23.3	6.1	70.6	7.3	8.6	27.9	42.4	6.6	0.0	3.8	3.5
48	SCA	25	R	0.069	0.014	8.14	24.9	52.6	20.0	27.4	8.3	9.6	29.5	34.8	6.9	0.1	3.0	7.9
49	SCA	25	R	0.202	0.218	3.03	19.9	18.3	6.3	75.4	11.3	9.1	27.3	32.2	12.0	0.2	5.4	2.5
50	MCA	15	B	0.145	0.065		19.6	30.3	10.8	58.9	14.9	8.4	11.4	24.2	22.7	0.0	5.5	12.9
51	MCA	15	F	0.028	0.008		56.4*	47.8	23.5	28.8	46.3	3.2	15.0	9.6	4.8	0.0	0.0	21.2
52	MCA	15	I	0.001	0.029		n/a*	73.8	-0.1	26.3	8.7	1.4	0.0	6.6	0.0	0.0	0.5	82.7
53	MCA	15	P	0.470	0.085	4.1	23.5	32.1	7.7	60.2	9.6	6.2	27.6	21.4	11.8	0.0	0.0	23.4
54	MCA	15	R	0.351	0.662	5.1	19.6	19.7	6.2	74.0	8.0	5.4	30.5	40.3	11.7	0.0	1.6	2.5
55	NA	16	B	0.089	0.150		21.1	72.1	5.4	22.5	51.0	7.4	10.4	4.7	4.6	0.0	5.2	16.7
56	NA	16	F	0.073	0.067		35.6	65.0	9.0	26.1	41.8	11.2	25.6	10.8	2.5	0.0	0.6	7.7
57	NA	16	P	0.221	0.267		13.3	68.0	7.1	24.9	27.4	22.4	9.9	14.4	9.4	1.6	7.7	7.1
58	NA	16	R	0.172	0.253		14.9	62.3	9.7	28.0	53.5	14.0	7.0	9.5	4.4	0.0	3.7	8.0
59	NA	17	B	0.043	0.023		39.3*	46.3	38.1	15.7	7.2	3.0	3.2	16.4	18.0	1.5	5.6	45.0
60	NA	17	I	0.016	0.220		90.5*	93.2	4.1	2.7	2.4	1.4	1.4	3.4	1.8	0.0	1.5	88.1
61	NA	17	I	0.072	0.151		36.5	61.6	6.3	32.1	24.7	5.3	32.9	19.8	4.0	0.0	0.3	13.0
62	NA	17	P	0.277	0.360		25.6	34.9	4.8	60.3	2.5	5.3	42.2	47.1	0.9	0.0	0.4	1.6

(*Continued*)

Tab.3 (Continued)

63	NA	17	R	0.763	0.826	1.9	21.5	35.4	3.4	61.3	0.0	0.0	59.0	40.3	0.7	0.0	0.0	0.0
64	NA	17	R	0.489	0.713		5.9	30.7	59.0	10.2	14.8	2.4	1.5	6.8	1.0	0.1	0.9	72.5
65	NA	18	B	0.096	0.087		33.3	31.7	9.8	58.5	26.4	5.7	27.2	20.1	8.3	0.1	4.2	7.9
66	NA	18	F	0.018	0.025		n/a	71.3	6.4	22.3	24.1	5.4	16.2	17.4	4.3	0.5	1.4	30.7
67	NA	18	I	0.002	0.018		n/a*	67.7	12.2	20.1	7.9	1.8	4.0	3.8	1.2	0.0	1.1	80.0
68	NA	18	P	0.340	0.095		21.9	39.5	5.7	54.9	1.0	1.4	38.2	54.5	2.8	0.0	0.0	2.1
69	NA	18	R	0.231	0.113		22.9	41.5	7.7	50.8	21.7	10.5	34.5	25.3	6.8	0.1	0.0	1.1
70	MW	19	B	0.181	0.071		15.1	56.9	9.0	34.1	8.0	21.3	1.4	48.7	7.7	0.0	0.7	12.2
71	MW	19	F	2.608	0.901	4.6	7.7	48.4	6.1	45.5	0.4	1.6	3.8	82.2	10.6	0.2	0.4	0.8
72	MW	19	I	0.014	0.006		76.0*	0.0	48.8	51.3	15.7	13.9	2.5	24.4	4.8	0.8	1.6	36.3
73	MW	19	P	0.277	0.333		8.3	49.5	16.7	33.8	13.6	11.6	0.0	32.4	3.5	0.2	5.8	32.8
74	MW	19	R	0.299	0.319		7.4	45.2	20.6	34.2	9.8	19.9	0.1	37.8	4.2	0.5	2.8	25.0
75	MW	19	R	0.223	0.291		11.2	47.2	5.0	47.8	13.8	19.6	8.0	48.8	5.1	0.2	1.7	2.9
76	MW	20	B	0.530	0.413		9.4	32.0	21.4	46.6	0.0	1.5	0.1	68.1	1.0	0.0	0.7	28.6
77	MW	20	F	0.143	0.024		13.3	32.1	35.9	32.0	27.3	6.0	1.6	16.6	7.8	0.0	2.4	38.4
78	MW	20	F	0.191	0.130		11.2	36.6	21.2	42.2	19.4	10.7	3.5	28.2	6.0	0.1	0.1	32.1
79	MW	20	I	0.019	0.041		54.9*	57.5	28.3	14.1	16.8	7.5	0.5	2.6	3.8	0.6	3.4	64.7
80	MW	20	P	0.758	0.613	0.5*	9.0	31.4	8.6	60.0	0.0	0.0	0.2	94.8	0.6	0.0	0.0	4.3
81	MW	20	R	0.577	0.317		9.7	32.7	11.1	56.2	7.7	19.6	2.9	45.4	2.8	0.0	1.3	20.2
82	W	23	I	n/a	0.231	n/a	n/a*	67.8	18.0	14.3	65.9	3.9	1.5	1.2	4.2	0.0	5.8	17.5
83	W	23	I	0.097	0.051		10.7*	30.6	58.7	10.6	6.3	1.3	0.0	2.2	0.0	0.0	0.0	90.3
84	W	23	I	0.176	0.164		8.3*	40.8	50.7	8.5	15.3	4.3	0.0	1.3	0.8	0.1	0.5	77.7
85	W	23	P	0.349	0.351		3.9*	5.8	68.0	26.2	1.4	0.9	0.0	0.2	0.1	0.0	0.1	97.3
86	W	23	P	0.268	0.215		4.1*	n/a	n/a	n/a	n/a	n/a	n/a	n/a	n/a	n/a	n/a	n/a
87	W	23	R	0.888	1.061		4.1	29.0	62.1	8.9	1.3	1.8	0.0	0.6	0.1	0.0	0.0	96.2
88	W	24	F	0.068	0.134		22.8*	70.9	9.8	19.3	37.0	7.1	0.2	10.7	5.5	0.2	0.1	39.1
89	W	24	I	1.547	1.492	24.9	6.6	30.7	2.9	66.4	0.6	1.3	0.0	3.0	94.6	0.4	0.0	0.0
90	W	24	I	0.052	0.051		21.1*	68.2	15.9	15.9	27.8	7.8	2.0	10.1	4.7	1.2	0.3	46.1
91	W	24	I	0.063	0.064		24.1*	53.0	20.0	27.0	23.6	2.8	0.0	7.5	4.0	1.7	2.3	58.1
92	W	24	R	0.165	0.195		11.8	43.7	14.0	42.3	14.6	7.8	0.4	19.5	20.4	1.8	0.0	35.5
93	W	24	R	5.361	5.312	3.5	3.2	12.3	70.2	17.6	0.3	0.2	0.0	5.7	0.0	0.9	0.0	93.0

*samples between LOD and LOQ
n/a*: data unavailable (these samples are between LOD and LOQ, and have very low/missing sample mass)
n/a: data unavailable
empty cells: samples below LOD

In summary, higher constituent masses are needed to surpass LOD/LOQ for TGA and FTIR, and thus higher total sample mass is favorable here. On the other hand, lower sample mass is more favorable for SEM-EDX. The relative agreement between results from each method as a function of sample mass can shed more light on these issues and design of sampling campaigns.

3.1 *Comparison of the mass-based FTIR and TGA*

Comparison of FTIR Q+K with TGA estimation of non-carbonates is shown in Figure 1a. As expected, these measures tend to increase together, though their ratio varies widely across

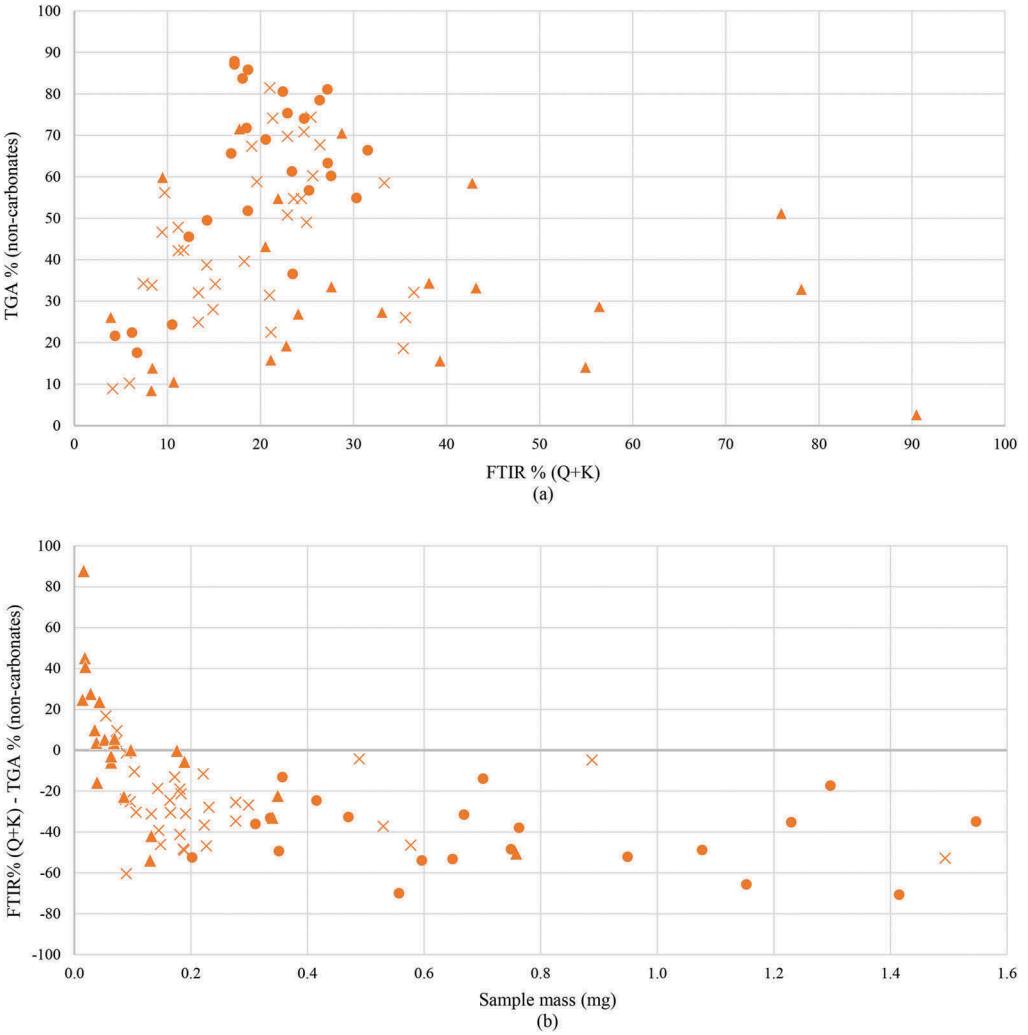

Figure 1. (a) Comparison of FTIR-based (Q+K) % versus TGA-based non-carbonate mineral mass % on corresponding PVC and PC replicate from each set collected in mines 10-25 (n=85). In 33 out of 93 samples, Q was below LOD, but K was above LOQ. (b) Difference between FTIR-based Q+K and TGA-based non-carbonate mineral mass % versus dust mass on each PVC replicate (n=83). The x-axis is capped at 1.6 mg since most of the data points are clustered in this range; 5 more data points exist between 1.6 - 8 mg, all following the observed trend. In both figures, × = either Q or K below LOD, ▲ = either Q or K between LOD and LOQ; • = both K and Q above LOQ.

the entire dataset (Figure 1a). For about 60% of the samples pairs, the TGA result is higher than the FTIR result (by a factor of 2-7x), whereas for another 15% of the pairs the FTIR result is higher than the TGA (by up to 4x). Figure 1b helps to illustrate the effect of sample mass here.

Based on higher-mass samples, for which both methods are expected to increase in accuracy, the tendency of the TGA result to be significantly higher than the FTIR result indeed suggests that quartz and kaolinite do not account for all of the non-carbonate mineral content in many of these respirable dust samples. Rather, based on the SEM-EDX results (Table 3), there appear to be other non-kaolinite alumino-silicates (e.g., feldspars or micas). Specifically, samples with high TGA overestimation of non-carbonates (compared to FTIR) have relatively very high SEM-EDX estimates of ASO. Further analysis of both the SEM-EDX elemental data and the FTIR spectra—in terms of potential peaks related to other silicates/minerals along with potential interferences—could provide useful insights on this topic and will be the focus of future work.

Figure 1b also clearly shows that low sample mass is correlated with observations of the FTIR result being higher than the TGA result. This is likely to be at least partly due to decreased analytical accuracy—and it is noteworthy that most of the low-mass samples in this study came from the intake and feeder locations (per Table 3). Based on SEM-EDX data, these samples often have relatively high carbonate (CB), coal and/or diesel particulate (C+MC) content, and thereby relatively low non-carbonate mineral content (ASK+ASO+S+SLO+M).

3.2 *Comparison of the FTIR and TGA to particle-based SEM-EDX*

Figure 2 shows the comparison between the FTIR and SEM-EDX results. As expected, results for FTIR derived Q and SEM-EDX derived S are in reasonable agreement (i.e., mean difference of about ±5%, with the exception of one outlier). That said, all but the outlier sample had <25% Q/S per either method, so the visual similarities between the two data series (in Figure 2) should be viewed accordingly.

Similar to the Q/S results, Figure 2 shows that FTIR K and SEM-EDX ASK results generally agree (mean difference of about 15%). Unlike the Q/S %, the K/ASK % ranged from ~0%

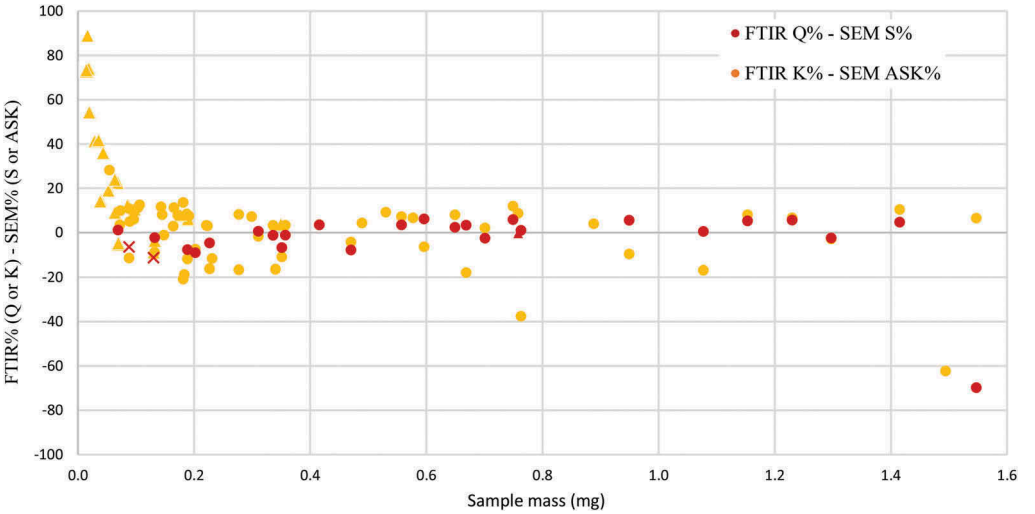

Figure 2. Difference between FTIR and SEM-EDX-derived mass % estimates for quartz/silica and kaolinite/alumino-silicates-kaolinite versus dust mass on each PVC replicate (n=33 for Q%-S%, n=83 for K%-ASK%). The x-axis is capped at 1.6 mg; 10 more data points exist (5 each for Q and K) between 1.6 - 8 mg, all following the observed trend. × = below LOD, ▲ = between LOD and LOQ; • = above LOQ.

up to ~90% per either method, so a mean difference of 15% can be considered to represent a good agreement. Similar to the comparison between FTIR and TGA, trends with sample mass are evident, with the lowest-mass samples likely being affected by accuracy issues. Considering there is reasonable agreement in K/ASK%, and ASK % is, on average, one-fourth of the total AS (i.e., ASK+ASO) per Table 3, it can be inferred there is indeed an abundance of non-kaolinite alumino-silicates in many of the samples. However, given the particle-based nature of the SEM-EDX analysis and the inordinately high AS content observed in many samples as mass increases, it is worth considering that other factors could be at play.

Figure 3 shows the comparison between the TGA and SEM-EDX results. In this case, all three primary components of the dust estimated by TGA (i.e., coal, carbonate, and non-carbonates) can be compared with results from SEM-EDX since its mineralogy classes can be loosely collapsed to match the TGA outputs per Table 1. The largest differences are again seen for the lowest-mass samples (typically in the I and F locations, per Table 3). Figure 3 suggests that these discrepancies are most often related to a tendency for the TGA to measure more coal (possibly including very fine diesel particulates not accurately counted in the SEM work) and less carbonate (possibly overcounted in the SEM work due to its coarser size, see Sarver et al. 2019) versus the SEM-EDX.

However, the effect of sample mass in Figure 3 is visibly diminished above about 100 µg. After that, in general, the SEM-EDX still tends overpredict non-carbonate minerals (mostly ASK+ASO+S per Table 3) versus the comparative measure, but to a lesser extent than observed in Figure 2. Frequently, this overprediction of non-carbonates by the SEM-EDX corresponds with an underprediction of coal (C+MC). Possible explanations for these results could be that coal particles are either impure, or are being coated (i.e., occluded) by relatively fine alumino-silicates, especially in the sampling locations where dust is actively being generated. Since the SEM-EDX effectively classifies particles based on their elemental content, whereas TGA classifies particles based on their mass, such occurrences could lead to significant differences between dust compositions indicated by these two methods. Notably, the fact that the carbonate results in Figure 3 (like the Q/S results in Figure 2) are in relatively good agreement provides some indication that high sample mass is probably not the only reason for high ASK+ASO content per SEM-EDX—meaning that particle interference effects due to loading are not alone responsible.

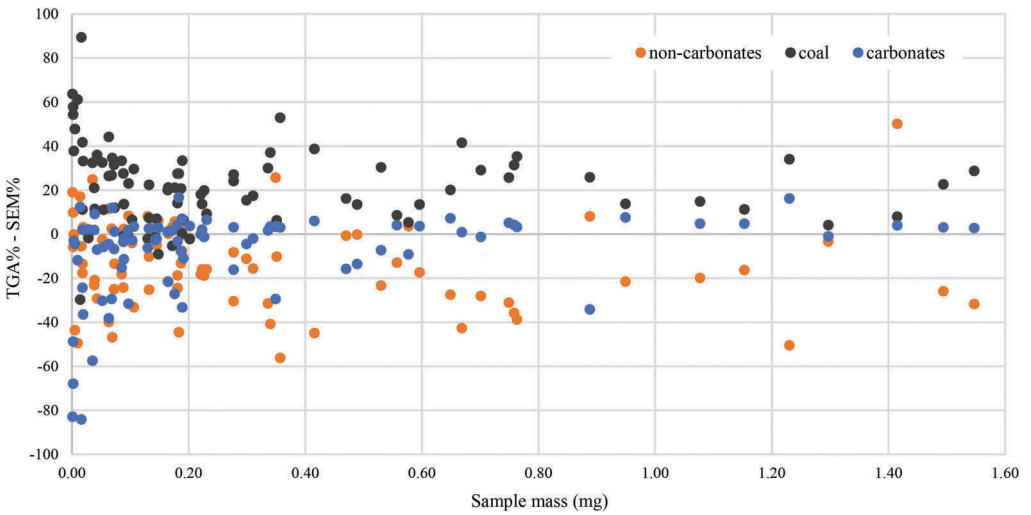

Figure 3. Difference between estimates of coal, carbonates, and non-carbonates mineral fractions derived from TGA and SEM-EDX results versus dust mass collected on each PVC replicate (n=91). The x-axis is capped at 1.6 mg; 5 sets of data points exist between 1.6 - 8 mg, all roughly following the observed trend.

4 CONCLUSIONS

For the first time, this study compared mineral content in respirable coal mine dust samples measured by FTIR, TGA, and SEM-EDX. Comparison of results from all three methods suggests the presence of significant non-carbonate mineral content other than quartz and kaolinite in the mine dust. Detailed analysis of the FTIR transmission and SEM-EDX elemental spectra might be valuable to better understand the specific mineral constituents. Further, results showed that the particle-based SEM-EDX frequently indicates much more mineral content (primarily other alumino-silicates) than is predicted by either of the mass-based measures. While sample mass/particle loading effects may be partly to blame, another possibility is that the SEM-EDX results are associated with impurity or occlusion of coal (or other particles) by fine alumino-silicates. While such particles may exhibit sufficient Si and Al to be classified as alumino-silicates by the SEM-EDX, their mass may be dominated by coal, resulting in very little accounting to the corresponding TGA and FTIR measures (non-carbonates and kaolinite, respectively).

Aside from comparison of results between analytical methods, this study also demonstrated the application of NIOSH's new DOF-FTIR method for research purposes—as opposed to personal exposure monitoring as it has been primarily intended. Results illustrate the usefulness of this method, specifically for determination of kaolinite content along with quartz, and should support continuing efforts to integrate the method into research and engineering studies.

ACKNOWLEDGEMENTS

This research was supported by funding from the Alpha Foundation for the Improvement of Mine Safety and Health and the US National Institute of Occupational Safety and Health. The authors gratefully acknowledge our many industry partners who provided mine access and logistical support for dust sampling. We also thank Mr. Alex Norris and Dr. Kyle Louk for their assistance with dust sampling, and Dr. Emanuele Cauda for his help with the FTIR data analysis. Views expressed here are those of the authors and do not necessarily represent the views of research sponsors or partners.

REFERENCES

Agioutanti, E. (2019) An improved TGA method for respirable coal mine dust and comparison to results by SEM-EDX. *Civil and Environmental Engineering*. Blacksburg, VA, Virginia Polytechnic Institute and State University.

Agioutanti, E., Keles, C. & Sarver, E. (2020) A thermogravimetric analysis application to determine coal, carbonate, and non-carbonate minerals mass fractions in respirable mine dust. *Journal of Occupational and Environmental Hygiene*, 17, 47–58.

Almberg, K. S., Halldin, C. N., Blackley, D. J., Laney, A. S., Storey, E., Rose, C. S., Go, L. H. T. & Cohen, R. A. (2018) Progressive Massive Fibrosis Resurgence Identified in U.S. Coal Miners Filing for Black Lung Benefits, 1970–2016. *Annals of the American Thoracic Society*, 15, 1420–1426.

Ashley, E. L., Cauda, E., Chubb, L. G., Tuchman, D. P. & Rubinstein, E. N. (2020) Performance Comparison of Four Portable FTIR Instruments for Direct-on-Filter Measurement of Respirable Crystalline Silica. *Annals of Work Exposures and Health*, 64, 536–546.

Blackley, D. J., Crum, J. B., Halldin, C. N., Storey, E. & Laney, A. S. (2016) Resurgence of Progressive Massive Fibrosis in Coal Miners. *Morbidity and Mortality Weekly Report*.

Castranova, V. & Vallyathan, V. (2000) Silicosis and coal workers' pneumoconiosis. *Environmental Health Perspectives*, 108, 675–684.

Cauda, E., Miller, A. & Drake, P. (2016) Promoting early exposure monitoring for respirable crystalline silica: Taking the laboratory to the mine site. *Journal of Occupational and Environmental Hygiene*, 13, D39–D45.

CDC (2006) Advanced Cases of Coal Workers' Pneumoconiosis — Two Counties, Virginia. *MMWR* 55.

IARC (1997) *Monographs on the evaluation of carcinogenic risks to humans: silica, some silicates, coal dust and para-aramid fibrils*., Lyon, France.
Johann-Essex, V., Keles, C., Rezaee, M., Scaggs-Witte, M. & Sarver, E. (2017a) Respirable coal mine dust characteristics in samples collected in central and northern Appalachia. *International Journal of Coal Geology*, 182, 85–93.
Johann-Essex, V., Keles, C. & Sarver, E. (2017b) A Computer-Controlled SEM-EDX Routine for Characterizing Respirable Coal Mine Dust. *Minerals*, 7, 15.
Laney, A. S. & Weissman, D. N. (2014) Respiratory Diseases Caused by Coal Mine Dust. *Journal of Occupational and Environmental Medicine*, 56, S18–S22.
Lee, T., Chisholm, W. P., Kashon, M., Key-Schwartz, R. J. & Harper, M. (2013) Consideration of Kaolinite Interference Correction for Quartz Measurements in Coal Mine Dust. *Journal of Occupational and Environmental Hygiene*, 10, 425–434.
Miller, A. L., Drake, P. L., Murphy, N. C., Cauda, E. G., Lebouf, R. F. & Markevicius, G. (2013) Deposition Uniformity of Coal Dust on Filters and Its Effect on the Accuracy of FTIR Analyses for Silica. *Aerosol Science and Technology*, 47, 724–733.
Miller, A. L., Drake, P. L., Murphy, N. C., Noll, J. D. & Volkwein, J. C. (2012) Evaluating portable infrared spectrometers for measuring the silica content of coal dust. *J. Environ. Monit*., 14, 48–55.
Miller, A. L., Weakley, A. T., Griffiths, P. R., Cauda, E. G. & Bayman, S. (2017) Direct-on-Filter α-Quartz Estimation in Respirable Coal Mine Dust Using Transmission Fourier Transform Infrared Spectrometry and Partial Least Squares Regression. *Applied Spectroscopy*, 71, 1014–1024.
MSHA (2008) Method No. P-7. Pittsburgh Safety and Health Technology Center.
NASEM (2018) *Monitoring and Sampling Approaches to Assess Underground Coal Mine Dust Exposures*, Washington, DC, The National Academies Press.
NIOSH (2019) FAST (Field Analysis of Silica Tool). Build 1.0.7.2 ed. Pittsburgh, PA, NIOSH-CDC.
Sarver, E., Keles, C. & Rezaee, M. (2019) Beyond conventional metrics: Comprehensive characterization of respirable coal mine dust. *International Journal of Coal Geology*, 207, 84–95.
Schatzel, S. J. (2009) Identifying sources of respirable quartz and silica dust in underground coal mines in southern West Virginia, western Virginia, and eastern Kentucky. *International Journal of Coal Geology*, 78, 110–118.
Su, X., Ding, R. & Zhuang, X. (2020) Characteristics of Dust in Coal Mines in Central North China and Its Research Significance. *ACS Omega*, 5, 9233–9250.